MNRAS 000, 1–12 (2019) Preprint 20 February 2024 Compiled using MNRAS LATEX style file v3.0

Classification and evolution of galaxies according to the dynamical state of host clusters and galaxy luminosities

D. F. Morell,[1,2]★ A. L. B. Ribeiro,[2] R. R. de Carvalho,[3] S. B. Rembold,[4]
P. A. A. Lopes,[5] A. P. Costa[2]

[1] *Observatório Nacional – MCTIC, Rio de Janeiro, RJ, 20921-400, Brazil*
[2] *Universidade Estadual de Santa Cruz, Laboratório de Astrofísica Teórica e Observacional, Ilhéus, BA, 45650-000, Brazil*
[3] *NAT - Universidade Cruzeiro do Sul / Universidade Cidade de São Paulo, 01506-000 Brazil*
[4] *Universidade Federal de Santa Maria, Santa Maria, RS, 97105-900, Brazil*
[5] *Observatório do Valongo, Universidade Federal do Rio de Janeiro, Rio de Janeiro, RJ, 20080-090, Brazil*

arXiv:2003.13836v1 [astro-ph.GA] 30 Mar 2020

Accepted XXX. Received YYY; in original form ZZZ

ABSTRACT

We analyze the dependence of galaxy evolution on cluster dynamical state and galaxy luminosities for a sample of 146 galaxy clusters from the Yang SDSS catalog. Clusters were split according to their velocity distribution in Gaussians (G) and Non-Gaussians (NG), and further divided by luminosity regime. We performed a classification in the Age-SSFR plane providing three classes: star-forming (SF), passive (PAS), and intermediate (GV – green valley). We show that galaxies evolve in the same way in G and NG systems, but also suggest that their formation histories leads to different mixtures of galactic types and infall patterns. Separating the GV into star-forming and passive components, we find more bright galaxies in the passive mode of NG than in G systems. We also find more intermediate faint galaxies in the star-forming component of NG than in G systems. Our results suggest the GV as the stage where the transition from types Sab and Scd to S0 must be taking place, but the conversion between morphological types is independent of the dynamical stage of the clusters. Analyzing the velocity dispersion profiles, we find that objects recently infalling in clusters have a different composition between G and NG systems. While all galaxy types infall onto G systems, Sab and Scd dominate the infall onto NG systems. Finally, we find that faint Scd in the outskirts of NG systems present higher asymmetries relative to the mean asymmetry of field galaxies, suggesting environmental effects acting on these objects.

Key words: evolution – galaxies: clusters: general – galaxies: formation – galaxies: groups: general

1 INTRODUCTION

Galaxy clusters are valuable laboratories to understand galaxy evolution in connection with the environment. In the hierarchical scenario, massive structures should be forming at the present epoch, as a result of mergers and accretion of less massive objects. Thus, clusters constitute complex systems in a wide range of dynamical and evolutionary states, usually reduced to two categories: virialized (or relaxed) and non-virialized (or non-relaxed) systems. Virialized clusters are expected to have nearly spherical shape and gaussian velocity distribution (e.g. Yahil & Vidal 1977; Faltenbacher & Diemand 2006), while non-virialized systems can show elongated shapes (Plionis 2004), non-gaussian velocities (e.g. Hou et al. 2009; Ribeiro et al. 2013a), and the presence of substructures (e.g. Roberts et al. 2018a; Lopes et al. 2018). Some works suggest that the way galaxies evolve is dependent on the dynamic state of their host clusters (e.g. Hou et al. 2009, 2012; Ribeiro et al. 2013a; de Carvalho et al. 2017, hereafter dC17), which underlines the importance of correctly determining the dynamic state of the clusters.

Different methods for assessing the relaxation degree of galaxy systems are found in the literature. For instance, detection of optical substructures (e.g. Hou et al. 2012; Wen & Han 2013; Cohen et al. 2015; Lopes et al. 2018; Soares & Rembold 2019), deviation of scale relations (e.g. Yang et al. 2010), merger signatures on images (e.g. Plionis et al. 2003; Allen et al. 2008; Million & Allen 2009), X-ray peak

★ E-mail: dailerfm@gmail.com

© 2019 The Authors

and BCG offset (e.g. Rossetti et al. 2016; Roberts et al. 2018a; Lopes et al. 2018; Foëx 2019), X-ray photon asymmetry and/or centroid shift (e.g. Ge et al. 2018; Roberts et al. 2018a; Bartalucci et al. 2019). In addition to these methods, the shape of the radial velocity distribution of cluster galaxies has been proved to be robust for separating relaxed from unrelaxed clusters, where "relaxed" means a system having member-galaxy velocity distribution roughly following the Maxwell-Boltzmann function (e.g. Ribeiro et al. 2013a, dC17). Recently, Roberts et al. (2018b) demonstrated that clusters with velocity distributions well fitted by a Gaussian have X-ray morphologies which are usually symmetric, whereas clusters with non-Gaussian velocity profiles show X-ray morphologies with significant asymmetries, suggesting the use of velocity distributions as a reliable way to determine cluster dynamical state.

When assessing Gaussianity in the radial velocity distribution, Gaussian and Non-Gaussian systems exhibit significant differences *wrt* some of their galaxy properties (Ribeiro et al. 2010, 2013a,b). For example, member galaxy luminosities are related to the dynamical state (e.g. Martínez & Zandivarez 2012; Wen & Han 2013), with non-Gaussian systems presenting a fainter characteristic absolute magnitude (Martínez & Zandivarez 2012). Also, non-Gaussian groups have larger velocity dispersions and, as a consequence, higher dynamical masses (Ribeiro et al. 2011; Old et al. 2018). In addition, less relaxed clusters show an increased star formation rate (Cohen et al. 2015; Roberts & Parker 2017), where faint galaxies are mainly find in the cluster outskirts, and being more metal rich, which can be interpreted as an evidence of preprocessing (dC17). Regarding the specific star formation rate (SSFR), Nascimento et al. (2019) find that the Gaussian passive population presents velocity segregation with luminosity. In addition, Soares & Rembold (2019) find lower mean stellar ages in unrelaxed clusters relative to relaxed clusters, and explain the differences between them as mainly driven by low-mass systems in the clusters outskirts, where substructures lies preferentially (e.g. Hou et al. 2012). These results suggest a connection between the dynamical state of clusters and the processes driving galaxy evolution, a link yet to be fully understood.

The cluster dynamical state is related to the orbits of member galaxies. As a galaxy moves through the cluster, its orbit is eventually modified, from highly radial trajectories in the cluster outskirts to circular orbits in central regions inside the virial radius. Along with galaxy dynamical history, physical properties also changes influenced by the cluster environment, and so can be linked to the orbital type. For example, different Hubble types are associated with different orbits, with early-type galaxies having more isotropic orbits than late-type galaxies (e.g. Tammann 1972; Sodre et al. 1989; Adami et al. 1998; Biviano et al. 2002; Aguerri et al. 2007; Cava et al. 2017; Mamon et al. 2019). The velocity dispersion profile (VDP) shape is also related to some properties such as the efficiency of merger activity and/or substructure (e.g. Menci & Fusco-Femiano 1996; Hou et al. 2012; Pimbblet et al. 2014; Bilton & Pimbblet 2018), presence of different spectral classes galaxies (Rood et al. 1972) and cluster dynamical state (e.g. Hou et al. 2009; Costa et al. 2018; Nascimento et al. 2019).

This paper is the fourth of a series in which we investigate the discrimination between Gaussian (G) and Non-Gaussian (NG) clusters, based on the velocity distribution of the member galaxies. First, de Carvalho et al. (2017) report evidence that faint galaxies in the outer regions of NG groups are infalling for the first time into the systems. Then, Costa et al. (2018) find significant differences between the velocity dispersion profiles (VDP) of G and NG system, and also regarding bright and faint samples of galaxies. Finally, the study of de Carvalho et al. (2019) on the Star Formation History (SFH) of cluster galaxies reveals that the SFH in faint spirals of NG groups is significantly different from their counterpart in the G groups, leading the authors to conclude that there is a higher infall rate of gas rich systems in NG groups.

In this work, we propose to investigate the evolution of cluster galaxies using the plane defined by the mean stellar age (hereafter, "Age") and specific star formation rate (hereafter, "SSFR") of galaxies to define their evolutionary stages. In §2 we define the cluster sample and describe their properties. Classifications in the Age-SSFR space and comparison of galaxy properties are performed in §3. In §4 we revisit the VDP problem, now splitting profiles according to our evolutionary classifications. Also in §4 we study the asymmetries of infalling galaxies onto G and NG systems. Finally, in §5 we summarize our results. Throughout the paper, were assumed the ΛCDM cosmology: H_0=72 km s^{-1}Mpc^{-1}, Ω_m=0.27 and Ω_Λ=0.73.

2 DATA

Our sample of galaxy clusters is defined from the Yang et al. (2007) (hereafter Y07) updated galaxy group catalog, constructed using a halo-based group finder optimized for grouping galaxies residing in the same dark matter halo (Yang et al. 2005).

2.1 General description

We briefly describe the data selection, which is the same as described by dC17 and Costa et al. (2018). Galaxies were retrieved galaxies from the Sloan Digital Sky Survey (SDSS; York et al. 2000) Data Release 7 within ±4000 km/s and up to 3 Mpc in projected distance around 344 Y07 group center coordinates, limited to $0.03 < z < 0.1$ and Petrosian magnitude $r < 17.77$. Galaxy membership was determined by the *shiftgapper* iterative technique (Fadda et al. 1996; Lopes et al. 2009), and relevant dynamical properties such as velocity dispersion, R_{200} and M_{200} were determined from the virial analysis (see details in Lopes et al. 2009). After the interloper elimination process, we consider two subsamples pertaining to different luminosity regimes. First we selected galaxies within $0.03 \leq z \leq 0.04$ and $-20.5 < M_r \leq -18.4$, which will be denoted as *faint* sample (F). The second subsample comprises galaxies with $0.04 < z \leq 0.1$ and $M_r \leq -20.5$, thus defining the bright sample (B). Some additional information were added from other available catalogs, which we briefly describe in the next paragraphs.

2.2 Additional information

We add some spectroscopic properties from SDSS tables performing a cross match by coordinates and inside a 0.5″ radius, using the CasJobs[1] platform. Thus, we retrieve the stellar masses and SSFRs for our sample from the *galSpecExtra* table (Kauffmann et al. 2004) corresponding to the *lgm_tot_p50* and *specsfr_tot_p50* parameters, respectively. A total of 84 objects without SSFR and/or age reliable measurements were discarded, and they represent only a small percentage (1.2%) of the whole sample. We also include the eclass spectral classification from the *SpecObj* table in the CAS, which is based on the first two expansion coefficients of the PCA decomposition for 170,000 SDSS spectra (Yip et al. 2004). The eclass parameter ranges from -0.35 to 0.5 for early- to late-type galaxies or AGN. Luminosity-weighted mean stellar ages and metallicities used in this work come from dC17, derived using the STARLIGHT code (Cid Fernandes et al. 2005). The errors of both stellar population parameters is assessed by dC17 in two different ways. First, the estimates are compared to those of Chen et al. (2012), based on Principal Component Analysis (PCA), and giving the following residuals relative to SDSS-DR12 values: ΔAge= 3.5 ± 2.7 Gyr; Δ[Z/H]= -0.01 ± 0.08. The second way is via repeated observations of the same galaxy from SDSS-DR7 (6148 repeated observations of 2543 galaxies), yielding a residual distribution with the following uncertainties: ΔAge= 0.0 ± 1.2 Gyr; Δ[Z/H]= 0.00 ± 0.04 (see more details in dC17).

We include morphological information for galaxies in our sample in two ways. First, we use the Domínguez Sánchez et al. (2018) catalog, which provides T morphological types for $\sim 670,000$ galaxies from SDSS, by training Convolutional Neural Networks (CNNs) with information from available sources such as Galaxy Zoo 2 (GZ2, Lintott et al. 2008; Willett et al. 2013) and the catalog of visual classifications provided by Nair & Abraham (2010). Secondly, we include the morphometric parameter G2, from the catalog of Barchi et al. (2020). This parameter is obtained applying the *CyMorph* algorithm on GZ2 galaxies, that uses the second gradient moments of the galaxy image to compute G2 (Rosa et al. 2018). We also add bulge, disk, and total stellar mass from the catalog of Mendel et al. (2013) for $\sim 660,000$ galaxies from the Legacy area of the SDSS DR7. These masses are based on a homogeneous catalog of g and r band photometry described by Simard et al. (2011) and extended with bulge+disk and Sérsic profile photometric decompositions in the SDSS u, i, and z bands. We also define a field sample, comprising 5997 galaxies, which is a result of stacking three catalogs available in the literature (Khim et al. 2015; Bradford et al. 2015; Fernández et al. 2015) in the SDSS DR7, DR8 & DR10 fields, respectively, and removing repeated objects and those belonging to galaxy clusters catalogs of Yang et al. (2007) and Tempel et al. (2017).

With all added information, we have a quite general characterization of the galaxies in our sample, in both photometry and spectroscopy.

[1] http://skyserver.sdss.org/CasJobs/

Table 1. Properties of the four subsamples to be studied. Median errors were determined as $0.7415(Q_{0.75} - Q_{0.25})$, where $Q_{0.25}$ and $Q_{0.75}$ are 25% and 75% probability quantiles, respectively.

Sample	N_{cl}	N_{gal}	$\log(M_{200}/M_\odot)$	R_{200}(Mpc)
GB	98	3662	14.45 ± 0.30	1.10 ± 0.25
NGB	26	1239	14.67 ± 0.53	1.23 ± 0.56
GF	12	699	14.38 ± 0.24	0.95 ± 0.19
NGF	10	1042	14.74 ± 0.31	1.32 ± 0.32

2.3 Dynamical state of clusters

Since we want to relate the galaxy properties with the dynamical state of the clusters, we add the classifications find by dC17, into Gaussian or non-Gaussian. dC17 assess the Gaussianity based on the Hellinger Distance (HD) (e.g. Huber 1981; Amari 1985) estimator over the cluster velocity distribution, establishing a reliability threshold depending on the cluster richness (see details in dC17). HD is a measure of the distance between two distributions, first introduced in astronomy by Ribeiro et al. (2013a), who demonstrate that HD overcomes other normality tests when comparing the amount of type I and II statistical error rates. Furthermore, dC17 compare HD with *mclust*, an independent method (see description in Section 3.1), obtaining similar results, although HD was find to perform slightly better. HD reliability is achieved for a richness of, at least, 20 galaxies, which translates in an additional total mass selection for our sample of $M > 10^{14} M_\odot$ (see dC17). This richness cut reduces the initial sample from 344 to 146 clusters, containing 6642 galaxies. In this work, we compare the properties of galaxies between Gaussian (G) and non-Gaussian (NG) systems, separating by luminosity regime Bright (B) or Faint (F), and thus defining the four subsamples to be analyzed subsequently: GB, NGB, GF and NGF. Table 1 shows the main properties of the defined subsamples.

3 CLASSIFICATION AND EVOLUTION OF CLUSTER GALAXIES

Although colors is widely used to identify populations of different degrees of star formation, it is well known that they suffer from degeneracy in age, metallicity and dust extinction (e.g. Gallazzi et al. 2005), and cannot represent low values of star formation rate (see e.g. Dressler & Abramson 2015). Cortese (2012), using UV and mid-IR star formation rates, conclude that optical colors alone are not able to distinguish between actively star-forming and passive galaxies. The use of NUV − r selection (e.g. Wyder et al. 2007) has the advantage of being model-independent at $z \approx 0$, but even at very low redshifts it remains difficult to correct the NUV flux for the effects of dust extinction in absence of detailed multi-band photometry (Belfiore et al. 2018). Besides, using UV − optical colors always reduces the sample size. In the case of our sample this reduction reaches $\sim 22\%$, since not all sources of SDSS have been observed by the *Galaxy Evolution Explorer* (GALEX).

Some authors overcome the color issue using the SSFR instead (e.g. Wetzel et al. 2012), which can show more sharply the degree of quiescence and galaxy bimodality. Furthermore, SSFR is a good proxy for the star formation history and the evolutionary stage of galaxies (e.g. Salim 2014;

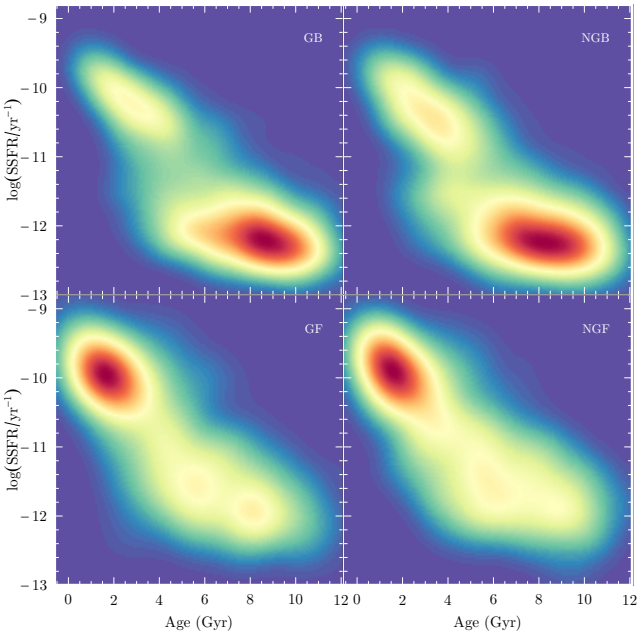


Figure 1. Density maps for GB, NGB, GF and NGF samples on the Age-SSFR plane. The density increases with color, from blue to red.

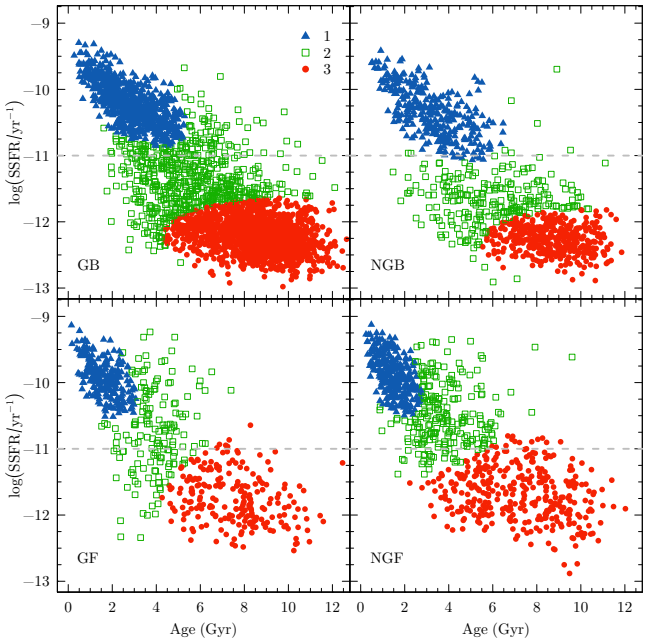


Figure 2. Classification given by *mclust* for 3 components in the Age-SSFR space, for each subsample. The horizontal dashed lines indicate the usual separator of active and passive galaxies given by Wetzel et al. (2012).

Brennan et al. 2015; Eales et al. 2017). In this work, in addition to SSFR, we also use the light-weighted age to characterize galaxy evolution.

3.1 The Age-SSFR plane

SSFR and mean stellar age are both bimodal properties of galaxies at low and medium redshifts (e.g. Kauffmann et al. 2003; Gallazzi et al. 2005; Wetzel et al. 2012). The former indicates the current star formation normalized by galaxy mass, and the latter is a tracer of the time elapsed since the last burst of star formation. Galaxies following the star forming main sequence (SFMS) are typically found at lower masses, while very low SSFR dominate the high-mass end. This behavior is often interpreted as galaxies growing along the SFMS at a rather constant SFR until they reach a critical stellar mass (or halo mass) threshold, above which they likely quench (e.g. Peng et al. 2010; Abramson et al. 2014). Considering that stellar mass represents the past star formation, then SSFR compares the current star formation to the averaged past one. If one assumes a constant SFR with time at low redshifts (e.g. Kennicutt Jr 1998) then SSFR scales as the inverse of the age of the galaxies. In the nearby universe the SSFR decreases when stellar mass increases, i.e., massive galaxies formed their stars in the past whereas less massive ones are more active in star formation, or equivalently, the mean age of the stellar populations of massive galaxies is higher than that of low mass galaxies (e.g. Li et al. 2011; Belfiore et al. 2018). This suggests a bimodal distribution with well separated peaks on the Age-SSFR plane, providing us a useful tool for classifying galaxies into evolutionary groups.

In Figure 1 we show the distributions of the four subsamples defined in the previous section (GB, NGB, GF, NGF) on this plane. In all panels we verify the expected bimodality, with well separated peaks with higher concentrations of old and low-SSFR objects in samples GB and NGB, with an inversion of this behavior in samples GF and NGF, as expected in the downsizing scenario (e.g. Neistein et al. 2006; Fontanot et al. 2009; Gu et al. 2018). Our first aim is to classify objects in this space. This is done using the *mclust* R code (Scrucca et al. 2016), that has been used successfully in astronomy (e.g. Einasto et al. 2012; Ribeiro et al. 2013a, dC17).

In model-based clustering, data is considered a mixture of densities. Each component in the mixture is modeled by the normal distribution which is characterized by its mean and covariance matrix. Briefly, *mclust* performs clustering by fitting Gaussian finite mixture models to the data, using an expectation-maximization algorithm, and further giving the number of optimal components via the lower Bayesian information criterion (BIC). We apply *mclust* to the whole sample choosing the more general covariance model "VVV" (varying volume, shape, and orientation), which returns the best gaussian mix being the one with three components. Considering that this is exactly the number of components we would intuitively expects ("blue", "red" and "green" family of galaxies) we test the robustness of such a finding. For each subsample, we run bootstrap realizations of the plane SSFR × Age one-hundred times fixing one quantity at a time. Fixing Age we find an outcome of three components 83% of the time and fixing SSFR, 91%. The subject of "clustering" in 2D is certainly a critical and important one and goes beyond the scope of the present investigation. However, the test we apply shows a consistency that matches the current vision of how galaxies evolve in the "SSFR × Age" plane.

The final classification groups are numbered as 1, 2 and

Table 2. Counts and median values of SSFR and Age for populations 1, 2, and 3 in the four stacked samples.

Counts				
Population	GB	NGB	GF	NGF
1	707	330	247	301
2	819	347	179	259
3	2071	544	265	437
log(SSFR/yr^{-1})				
Population	GB	NGB	GF	NGF
1	-10.2±0.4	-10.4±0.4	-9.9±0.3	-9.9±0.3
2	-11.4±0.4	-11.7±0.3	-10.8±0.6	-10.6±0.5
3	-12.2±0.3	-12.3±0.2	-11.8±0.4	-11.7±0.4
Age (Gyr)				
Population	GB	NGB	GF	NGF
1	2.9±1.4	3.2±1.5	1.7±0.8	1.5±0.7
2	5.4±1.9	5.6±1.9	4.0±1.0	3.7±1.3
3	8.5±1.8	8.5±1.6	7.5±1.8	7.1±2.3

3 for blue, green and red points of Figure 2, respectively, where we also present lines separating star-forming and passive subsamples according to log(SSFR/yr^{-1}) = −11 (Wetzel et al. 2012). Looking at population 3 (red points) we see that the Age range for both bright and faint galaxies in G systems is the same, extending to ∼4 Gyr, but for NG systems this does not happen. While the bright sample extends to ∼6 Gyr, the faint sample extends to younger ages, ∼2 Gyr, indicating recent episodes of star formation in this type of objects. Still in this figure, note that galaxies in population 1 (blue points) are distributed in the same way *wrt* luminosity, irrespective of the dynamic state of the host clusters. The bright samples (G and NG) have population 1 with Age $\lesssim$ 6 Gyr, while the faint samples (G and NG) have younger population 1, with Age $\lesssim$ 3 Gyr.

Counts and median values of SSFR and Age for populations 1, 2, and 3 in the four stacked samples are presented in Table 2, where we see a clear progression of young and high-SSFR objects to older and low-SSFR objects, passing through an intermediate population of galaxies. This sequence has statistical support from the Kruskal-Wallis (KW) test from the *pgirmess* R package (Giraudoux 2018). The KW test is used to compare two or more populations and tests the null hypothesis that all populations have equal distribution functions against the alternative hypothesis that at least two of the populations have different distribution functions (Corder & Foreman 2009). Importantly, the KW test corrects non-complementarities, making it very powerful when comparing more than two samples simultaneously. The test finds significant difference at the 95% confidence level between the populations ($1 \times 2 \times 3$), irrespective of being G or NG, B or F. This result indicates that the sequence $1 \rightarrow 2 \rightarrow 3$ can be understood as a physical transition of star forming (SF) to passive galaxies (PAS), passing through the green valley (GV) (Martin et al. 2005). On the other hand, there seems to be no significant difference between samples G and NG, only between B and F galaxies. Indeed, from Table 2, we see that the differences in age and SSFR between objects of the same class in G and NG systems are less than the sum of the errors in quadrature around their medians. In the same table, we see large differences in counts between all samples.

Computing the fractions of galaxies in populations 1, 2 and 3, we find (20% ± 2%, 23% ± 3%, 57% ± 2%) and (27% ± 2%, 28% ± 3%, 45% ± 2%) for the GB and NGB samples, respectively. Hence, for bright galaxies, the proportion of SF + GV objects is higher in NG systems **(55% ± 4%)** than in G systems **(43% ± 3%)**, and PAS galaxies are dominant in G systems. On the other hand, the proportions find for faint objects are all similar: (36% ± 2%, 26% ± 3%, 38% ± 2%) and (30% ± 2%, 26% ± 4%, 44% ± 3%), for the GF and NGF samples, respectively. This leads us to a first finding: galaxies seem to evolve the same way in all samples, following the sequence $1 \rightarrow 2 \rightarrow 3$, but the mixtures of types differ between GB and NGB systems. To better understand this result, we need to further investigate the intermediate population, and also use a wider set of properties to evaluate in detail the differences and similarities between the stacked samples.

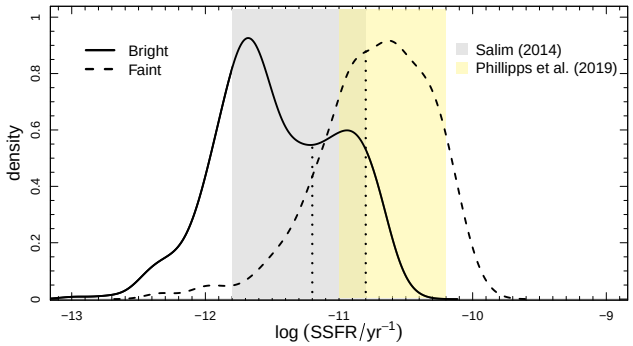


Figure 3. Distributions of SSFR for group 2 objects. Delimiters of GV galaxies from Salim (2014) and Phillipps et al. (2019) are indicated in gray and yellow, respectively. Vertical dotted lines indicate the separation between passive and star-forming galaxies in each sample.

3.2 The intermediate population

In Figure 2, we note that population 2 consists of a mixture of star-forming and passive objects, allowing a further characterization of the intermediate galaxies. We also notice that the line log(SSFR/yr^{-1}) = −11 divides galaxies differently, especially in samples B or F. In Figure 3, we present the SSFR distribution of bright and faint galaxies only in population 2. The B sample presents a clear bimodality while the F sample is a single broad mode. Typical GV delimiters of Salim (2014) and Phillipps et al. (2019) are shaded in gray and yellow, respectively. Note that the B sample is better delimited by the boundaries of Salim (2014), while the F sample is better framed by the delimiters of Phillipps et al. (2019). These features indicate that transitional objects are not homogeneous in luminosity. Using *mclust*, we separate star-forming and passive modes of B galaxies at log(SSFR/yr^{-1}) ≈ −11.2, see Figure 3. As a consequence, population 2 is separated differently between the samples: 61% ± 4% (39% ± 5%) of passive (SF) for GB; and 82% ± 4% (18% ± 6%) for NGB. Recall, from Section 3.1, the higher fraction of population 2 galaxies in the NGB sample (33%) than in the GB sample (23%). These differences are significant at the 95% confidence level, according to the *twoSamplePermutationTestProportion* function implemented in the EnvStats R package (Millard 2013), which performs a two-sample permutation test to compare two proportions.

Regarding F objects, we split them at the median, $\log(\mathrm{SSFR/yr^{-1}}) \approx -10.8$, see Figure 3. The resultant mixtures have the following proportions: 40% ± 5% of passive and 60% ± 4% of star-forming galaxies for GF; and 22% ± 7% of passive and 78% ± 4% star-forming galaxies for NGF. Hence, faint galaxies in GV are dominated by star-forming galaxies, but there are more passive objects in the GF sample, and more star-forming objects in the NGF sample. This is the opposite of what happens with bright galaxies. This result may be related to the work of de Carvalho et al. (2019) who find that faint spirals of NG groups are significantly different from their counterpart in the G groups, regarding their star formation history.

3.3 A physically intermediate population?

The results presented in the previous section show that intermediate galaxies correspond to different mixtures of passive and star-forming type objects depending on the sample. It is important to assess whether population 2 is in fact physically intermediate or corresponds to a mixture of types indistinguishable from those of populations 1 and 3, composing a kind of "purple" population (see Mendez et al. 2011). To investigate this point we use a selected set of parameters that allow a more general characterization of our samples. We first choose parameters linked to the structure of the galaxies (the B/T ratio, the Sérsic index – n_g, and the bulge mass, from Mendel et al. (2013). The behaviour of these parameters with respect the sequence SF $\rightarrow GV_1 \rightarrow GV_2 \rightarrow$ PAS is shown in the upper row of Figure 4. GV1 and GV2 denote the star-forming and passive components of the green valley, defined in Section 3.2. As expected, we see increasing values of all parameters along the sequence. But note that galaxies in the GV present intermediate values, agreeing with results reported by other authors (e.g. Schiminovich et al. 2007; Mendez et al. 2011; Coenda et al. 2018). We also see a significant separation between the trends for objects in samples B and F. Mass and size of objects are likely behind this result, since they increase along the sequence, and thus affect the structural parameters.

In the middle row, we present the behaviour of three morphological parameters that are defined and computed differently. The well known T-Type and eclass[2], plus G_2. The parameter G_2 is the second gradient moment within the GPA (Gradient Pattern Analysis) formalism (Rosa et al. 1999; Andrade et al. 2006; Rosa et al. 2018; Barchi et al. 2020). After a comparative analysis considering other morphometric parameters, Rosa et al. (2018) find that G_2 is the one with best performance (90% success) to separate elliptical and spiral galaxies, motivating our choice to use it.

Looking at Figure 4, we see that T-Type presents a similar behavior in all samples, except for a few fluctuations. At the same time, eclass separates samples B and F, with the paths well apart at the beginning of the sequence (SF) and identical at the end (PAS). Finally, the parameter G2

[2] Actually, eclass is the monoparametric spectral classification based on the eigentemplates expansion of galaxy's spectrum, whose values are correlated with galaxy morphology, from about −0.35 for early-type galaxies to 0.5 for late-type galaxies (Yip et al. 2004).

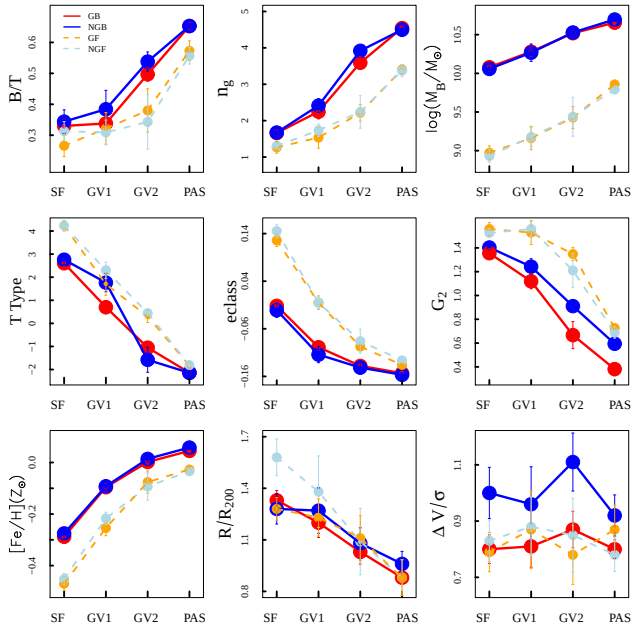


Figure 4. Evolutionary sequence for properties B/T, n_g, M_B, T, eclass, G_2, [Fe/H], R/R_{200}, and $\Delta V/\sigma$. Samples and tracks are indicated by colors red (GB), blue (NGB), orange (GF), and light blue (NGF). Solid and dashed lines depict bright and faint samples, respectively. SF indicates star-forming galaxies, GV1 and GV2 denote the star-forming and passive components of the green valley, and PAS indicates passive objects. Error-bars are obtained from a bootstrap technique with 1000 resamplings.

also shows a separation between samples B and F, but with some differences. First, the paths are less separated at the SF stage. Second, samples GF, NGF and NGB are similar at the end of the sequence (PAS), but note that the behavior is distinct at the GV2 and PAS stages for galaxies in the GB sample, compared to the NGB sample. This difference means that G systems contain a higher fraction of bright galaxies among the GV2 and PAS populations, than NG systems.

In the lower row of Figure 4 we first see metallicity presenting separated paths *wrt* the luminosity of the objects (B × F), following the mass-metallicity relation. Still in the lower row, we see that the projected clustocentric distance, R/R_{200}, behaves the same way for all but one sample, NGF, which presents a more peripheral distribution of SF and GV1 objects. Finally, we present the behavior of the normalized velocity offsets, $\Delta V/\sigma$, which refer to the cluster median velocities ($\Delta V = V_{gal} - V_{cluster}$), and are scaled by the cluster velocity dispersions (σ). The velocity offsets have a flat behavior along the evolutionary sequence, although the NGB sample presents higher velocities, suggesting a distinct kinematic behavior, possibly linked to disturbances experienced by NG clusters (Ribeiro et al. 2013a; de Carvalho et al. 2017).

Except for velocities and B/T, all other properties in Figure 4 have significant differences between one stage of evolution and another (within each sample). This has the statistical support of the Conover test (Conover 1999), from the *DescTools* R package (Signorell et al. 2016). This test performs a multiple comparison between the datasets and

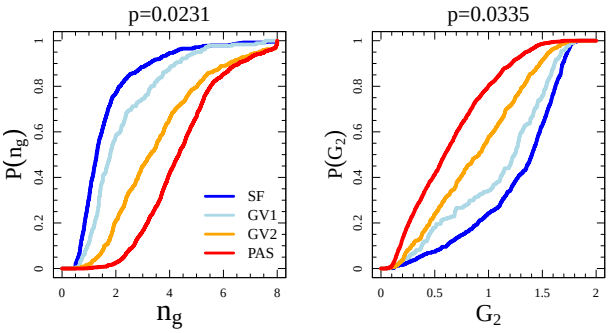


Figure 5. Example of the Conover test diagnostics for the cumulative distribution function of the Sérsic index and the G2 parameter for galaxies in GB systems. Curves are indicated by colors red (GB), blue (NGB), orange (GF), and light blue (NGF).

verifies whether the cumulative distribution function (CDF) of one does not cross the CDF of the other at the 90% c.l. As an example, we show in Figure 5 the Conover test diagnostics for the cumulative distribution function of the Sérsic index, n_g, and the G2 parameter for galaxies in GB systems. Note in this figure that curves for GV1 and GV2 are not coincident with those for SF and PAS, respectively. The outcome not only reinforces the idea of an evolutionary sequence, but it also means that SF galaxies are different from GV1 and PAS objects are distinct from GV2, for seven (of nine) properties studied in this work. This result may indicate that galaxies in GV are not just a "purple" mixture of bulges and disks, but actually correspond to objects at an intermediate stage of their evolution.

3.4 Morphological trends

In the previous section, we find a small (but significant) morphological difference between GB and NGB systems at the GV2 and PAS stages, according to parameter G2. This indicates that G systems contain a higher fraction of early-type galaxies in the GV2 and PAS populations compared to NG systems, or could mean that morphological transformation times are shorter in G clusters for bright galaxies. This can be better understood if we study how morphological types are distributed in these systems. Using information from Domínguez Sánchez et al. (2018) catalog, we present in Figure 6 the fractions of galaxy types E, S0, Sab, and Scd along the evolutionary sequence introduced in the previous sections. In this analysis, we remove all objects without reliable classification, which represent ~19% of the whole sample.[3]

In panel (a) of Figure 6, we see the expected increasing of the elliptical fraction in all samples, with different paths for B and F samples, and a high fraction of ellipticals allocated in GB and NGB systems at GV2 bin, compared to GF and NGF systems. The result indicates a dichotomy in the formation of ellipticals *wrt* their luminosities. We draw attention to the transition GV1 → GV2, much more

[3] The removal does not significantly modify the distribution of galaxy types defined in Section 3.1 among the four samples under study.

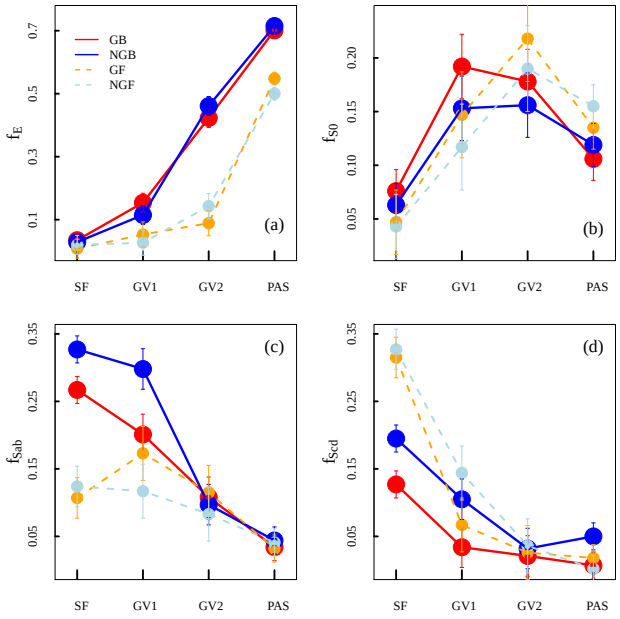


Figure 6. Fractions of galaxy types E, S0, Sab, and Scd along the evolutionary sequence SF → GV_1 → GV_2 → PAS. Samples and tracks are indicated by colors red (GB), blue (NGB), orange (GF), and light blue (NGF). Solid and dashed lines depict bright and faint samples, respectively. SF indicates star-forming galaxies, GV1 and GV2 denote the active and passive components of the green valley, and PAS indicates passive objects.

pronounced for bright galaxies, revealing the importance of transformations through the GV to separate the paths of bright and faint objects.

On panel (b), we see that galaxies S0 types are more frequent among GV galaxies than among SF and PAS galaxies. Actually, GV1 is dominated by S0 and Sab types, while GV2 is dominated by S0 and E, considering all the panels in the figure. This suggests evolution through the GV, and that S0 type is crucial for understanding the transition from late to early type objects, in agreement with recent works (e.g. Bait et al. 2017; Bremer et al. 2018). At the same time, the fraction of Sab decreases from SF to PAS. It should be noted, on panel (c), that the Sab fraction is higher in bright samples at the SF and GV1 bins, and that the NGB sample has the highest fraction of these objects. Indeed, the fraction of Sab galaxies in NGB systems, f_{Sab}^{NGB}, has a small drop over the SF → GV1 transition, and a significant drop during GV1 → GV2. This is accompanied by a significant growth in the fraction of S0 objects in these systems, f_{S0}^{NGB}, over SF → GV1, and just a small growth fraction over GV1 → GV2. For galaxies in GB systems we see a similar behaviour, but note that the decrease in the fraction of Sab galaxies in GB systems, f_{Sab}^{GB}, during the same transitions (SF → GV1 and GV1 → GV2), is lower, suggesting that environmental effects are somehow regulated by the dynamic state of the clusters. Still in panel (c), we see that there is no significant reduction of faint objects over SF → GV1, and only a modest decrease over GV1 → GV2. This suggests that, in the case of low luminosity galaxies, Sab objects do not decrease enough to achieve the S0 growth observed in panel

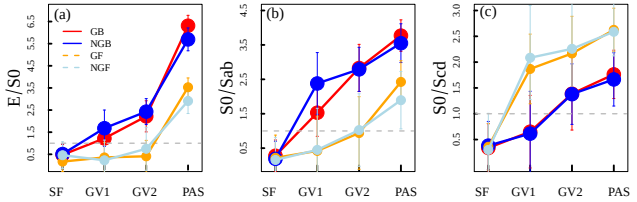


Figure 7. Number ratios E/S0, S0/Sab, and S0/Scd along the evolutionary sequence SF $\rightarrow$ GV$_1$ $\rightarrow$ GV$_2$ $\rightarrow$ PAS. Samples and tracks are indicated by colors red (GB), blue (NGB), orange (GF), and light blue (NGF). Solid and dashed lines depict bright and faint samples, respectively. SF indicates star-forming galaxies, GV1 and GV2 denote the active and passive components of the green valley, and PAS indicates passive objects. Dashed lines indicate equal counts of the morphological types.

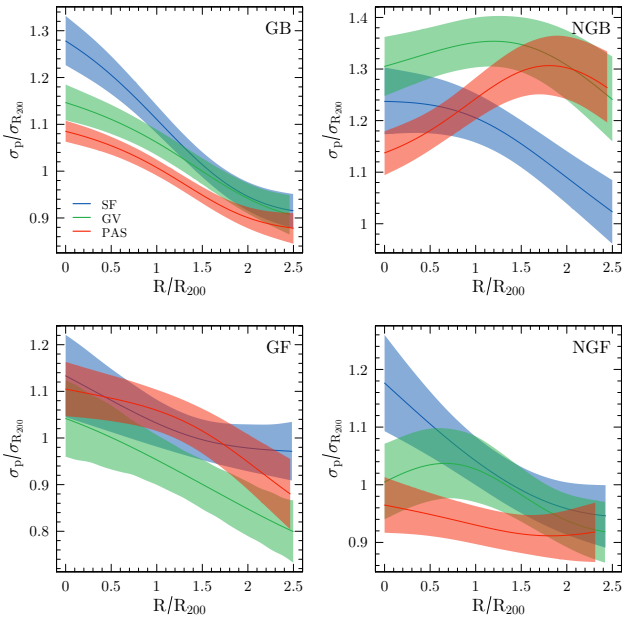


Figure 8. VDPs for our four subsamples, using the Bergond et al. (2006) prescription. Colors correspond to evolutionary classifications. Shaded area represents the 1σ confidence interval.

(b). This brings us to panel (d), where we see the impressive decrease of faint Scd objects during the aforementioned transitions, indicating that the S0 growth in F samples is correlated with the depletion of Scd galaxies both in G and NG systems. We still highlight in panels (c) and (d) an important difference in the proportion of types Sab and Scd at the SF bin. While the proportion of Sab objects is much higher for bright galaxies, the proportion of Scd objects is much higher for the faint ones, indicating that the bulk of the star forming main sequence corresponds to Sab or Scd types, depending on the luminosity range of the sample.

As a general result, the fractions of galaxies E increases while those of Sab and Scd decrease along the sequence SF $\rightarrow$ GV$_1$ $\rightarrow$ GV$_2$ $\rightarrow$ PAS. Reducing a population means transformation or destruction of individual objects. Increasing a population means receiving a new contingent or having other populations within the clusters being converted to that one. But new contingents via infall do not seem sufficient to recover the Sab and Scd galaxy counts. Also, recall that GV1 is dominated by a mixture of S0 and Sab, while GV2 is more populated by S0 galaxies (and E galaxies in GB and NGB samples). At the same time, there is a significant increase in S0 counts concomitant with a drop in Scd objects for faint galaxies from SF to GV2. Finally, ellipticals dominate the PAS subsample with a drop of S0 objects. Despite the details of this morphological balance, these facts suggest the GV as the stage of galaxy evolution where the transition from types Sab and Scd to S0 must be taking place, and that some S0 are converted into ellipticals. This view agrees with the scenario proposed by Bait et al. (2017), where the fraction of early-type spirals decreases towards the green valley from the blue cloud, coinciding with the increase in the fraction of S0 due to environmental effects. Our results add to this scenario that the fraction of faint late-type spirals also decreases accompanied by an increase of the fraction of faint S0 galaxies.

In Figure 7 we reinforce this view presenting the number ratios of morphological types E/S0, S0/Sab, and S0/Scd. On panel (a) we see that the E/S0 ratio is increasing along the sequence, but notice that the growth rate is higher for bright galaxies, for which the ratio E/S0 > 1 at the GV1 stage, while for faint galaxies this only happens after GV2. This suggests that the S0 $\rightarrow$ E conversion is regulated by galaxy luminosity. On panel (b) we see a similar behavior regarding the conversion Sab $\rightarrow$ S0. In this case, note that the S0/Sab > 1 during the SF $\rightarrow$ GV1 transition for bright galaxies, while for faint galaxies this happens at the GV2 stage. Finally, we see in panel (c) that S0/Scd > 1 over the SF $\rightarrow$ GV1 transition, for faint galaxies, while this happens over GV1 $\rightarrow$ GV2, for bright galaxies. We highlight the strong dependence on galaxy luminosities regarding the conversions between morphological types. It is worth mentioning that conversion of one morphological type into another seems to be independent of the dynamical stage of the clusters, namely, the behaviors for E/S0, S0/Sab, and Scd are similar for G and NG systems.

4 VELOCITY DISPERSION PROFILES

Galaxy classes and morphological changes should be related to galaxy orbits. In this section we complement the analysis of the distinction between the evolutionary classes and morphologies from the dynamical point of view, comparing their radial velocity dispersion profiles (VDPs) in each sample as established before: GB, GF, NGB and NGF. The analysis of the VDPs is useful to indicate the degree of orbital segregation between the different evolutionary classes. The VDPs are constructed using the Bergond et al. (2006) definition, with the Gaussian window function corrected by Bilton & Pimbblet (2018). The window size was set to be the bi-weight scale estimator from Beers et al. (1990) for the values of the projected radii, thus overcoming the dependence on a somewhat arbitrary value, as used by other authors before (see Bilton & Pimbblet 2018). For each bin of R/R$_{200}$ the dispersion and the corresponding 1σ confidence interval are determined from 1000 bootstrap realizations using the robust bi-weight estimators of location and scale from Beers

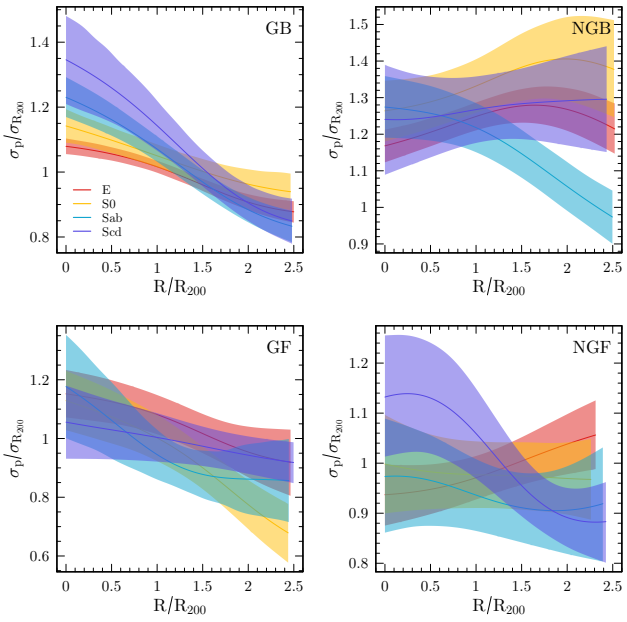


Figure 9. VDPs for our four subsamples, using the Bergond et al. (2006) prescription. Colors correspond to morphological types. Shaded area represents the 1σ confidence interval.

et al. (1990). Then, the VDPs were normalized by R_{200} and the velocity dispersion of the corresponding cluster.

4.1 VDP results

In Figure 8 we observe that, for bright galaxies in G systems, VDPs for each evolutionary class are similar in shape, presenting a monotonic decreasing behaviour, typical of systems relaxed in the center plus a radial component from infalling objects (e.g. Mohr et al. 1996; Biviano & Katgert 2004; Costa et al. 2018). Although the VDPs merge at large radii, they are separated in the inner cluster regions, $\lesssim 1.5\,R_{200}$, with SF, PAS and GV galaxies presenting higher, lower and intermediate velocity dispersions, respectively, which may be indicating different infall times for these populations. Faint galaxies in G systems also present decreasing VDPs, but significantly entangled at all radii possibly because these galaxies have similar infall times with different levels of preprocessing, although the poorer statistics compared to the bright galaxies hampers a more sound conclusion.

A different picture can be seen for NG systems. For bright galaxies, the SF population still presents a monotonic decreasing VDP, but both the GV and PAS populations now present increasing VDPs up to $\sim 1.5\,R_{200}$, which may be indicating the presence of dynamic disturbances (Menci & Fusco-Femiano 1996; Bilton & Pimbblet 2018).[4] As showed by Fitchett & Webster (1987) interactions and substructures could modify the velocity dispersion profile in the central cluster region. In this case, a possible scenario is to assume that the time scale of the dynamic disturbance is shorter than the infall time of SF galaxies, which do not present the central inversion of the VDP. In that context, note how passive galaxies is the most affected, with a marked inversion of the VDP, compared to that of the GV population. Still considering the VDP for NGB systems, we should mention that the depression around $1.0\,R_{200}$ observed by Costa et al. (2018) possibly results from the superposition of the VDPs of SF, GV and PAS populations. Finally, faint galaxies in NG systems present the following composition: SF with decreasing VDP, accompanied by a slightly declining (almost flat) VDP of PAS galaxies, and a disturbed VDP of GV galaxies. This case is more complex, since we have an approximate flat component, usually associated with objects in completely isotropic orbits (see Girardi et al. 1998), combined with a disturbed GV.

We can better understand the VDPs shown in Figure 8 if they are reconstructed for the morphological types E, S0, Sab and Scd. This is presented in Figure 9, where we clearly see, for GB systems, the gradation of profiles from that with the largest isotropic component (E galaxies) to the one with less isotropic orbit contribution (Scd galaxies). GF systems still present overlapping profiles that are not very enlightening for the discussion. On the other hand, VDPs for NGB systems reveal that the component with decreasing profile, previously associated to SF objects, corresponds to Sab galaxies, and this is the component that may be dominating the infall, after the others have experienced some dynamical interaction. At the same time, for NGF systems, we see the only component with decreasing profile corresponding to Scd galaxies, while S0 and Sab galaxies present flat VDPs, and E galaxies have an inverted profile, possibly being the only disturbed component of the system. Since more evolved galaxies are also the ones that have been in the clusters for the longest time, we expect them to show signs of a dynamic disturbance before the other components, especially those that still enter the system in radial orbits. This could explain the undisturbed behavior of Sab and Scd galaxies in NGB and NGF systems, respectively.

4.2 Asymmetry of infalling galaxies

We must point out that bright galaxies infalling into NG systems are largely Sab, and that in the bright regime there is more conversion of Sab objects into S0, as we find in Section 3.4. In contrast, faint galaxies infalling into NG systems are typically Scd, and that in the faint regime there is more conversion of Scd objects into S0. This suggests a connection between galaxy interacions during the infall and the transformation of late type galaxies into S0. In the cluster environment several mechanisms (ram-pressure, harassment, starvation, etc.) can operate to start the transition of spirals to S0 (see e.g. Boselli & Gavazzi 2006; D'Onofrio et al. 2015, and references therein). Disentangling these non-excluding mechanisms is beyond the discussion raised in this work, which is looking for differences between G and NG systems.

We use the asymmetry of galaxies as an indicator of interaction effects. Asymmetry is measured using the correlation between the original and rotated image with the code *CyMorph* (see Rosa et al. 2018). Regarding bright Sab galaxies, we find no difference between G and NG systems *wrt* bright Sab in the field. For faint Scd we find an excess of asymmetry in NG systems. This is shown in Figure 10,

[4] Other possibility is circularization due to the two-body relaxation, but this is efficient only in the very central regions of clusters (see e.g. Girardi et al. 1998).

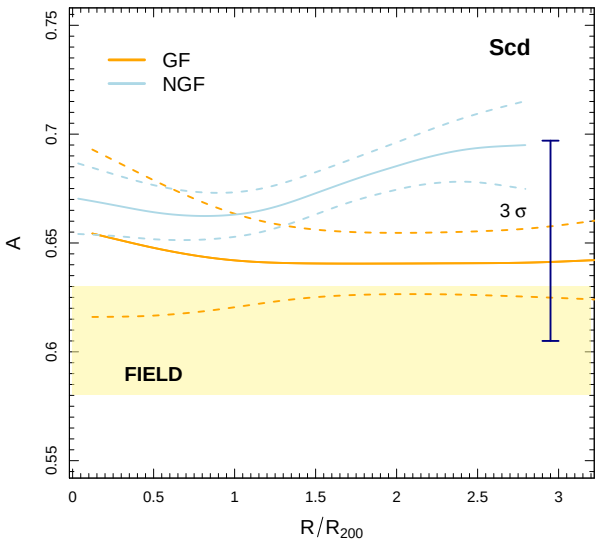


Figure 10. Asymmetry parameter for faint Scd galaxies in G and NG systems. Shaded areas indicate mean plus 1σ asymmetries of Scd galaxies for a field sample in the same luminosity regime. Dashed lines indicate the 1σ confidence interval.

where the shaded area indicates typical asymmetries of Scd galaxies for a field sample in the same luminosity regime as our faint samples. We should note a slight difference between faint Scd in G systems and Scd galaxies in the field (yellow shaded area). At the same time, faint Scd in NG systems present asymmetries varying from $\sim 2\sigma$ at $1R_{200}$ to $\sim 3\sigma$ at $3R_{200}$ above the mean asymmetry in the field, suggesting they may be experiencing interactions that affect their shape. For low-mass galaxies, morphological transformation can be associated with minor mergers during the infall. In fact, Moss (2006) shows that $\sim 50-70\%$ of the infall population are found to be in merging systems and slow galaxy-galaxy encounters. Roberts et al. (2019) propose a slow-then-rapid scenario of satellite quenching, with the low-quenching portion being consistent with quenching via steady gas depletion and the rapid-quenching portion being consistent with ram-pressure stripping completing the quenching of low-mass satellites. Other possible mechanism is the harassment, which is characterized as the combined effect of tidal interactions between infalling galaxies and the global cluster potential, and of the tidal interaction with close high-speed encounters with other cluster members (Moore et al. 1996).

5 SUMMARY

In this work, we classify galaxies in the Age-SSFR space using the *mclust* code. The procedure leads to three galaxy populations: young with high SSFR (SF), old with low SSFR (PAS), and an intermediate population (GV). Our aim is to find differences between these populations in the four samples of galaxies divided according to the dynamic state of their host clusters (G or NG) and the luminosity of the objects (B or F). Our main results are:

(1) Bright galaxies differ with respect to the populations identified in the Age-SSFR space. There are more bright SF + GV galaxies in NG (55% ± 4%) than in G systems (43% ± 3%). We also find more bright passive galaxies in G (57% ± 2%) than in NG (45% ± 2%) systems. Also, galaxies in GF and NGF samples present similar proportions of types SF, GV, and PAS.

(2) The comparison of populations identified in the Age-SSFR space indicates strong difference between the populations (SF,GV,PAS), but weak or null difference between the samples G and NG, indicating that galaxies quench in the same way independently of the dynamical state of the clusters.

(3) Separating the intermediate population (GV) into star-forming (GV1) and passive components (GV2), we find more bright galaxies in the passive mode of NG (82% ± 4%) than in G (61% ± 4%) systems. We also find more intermediate faint galaxies in the star-forming side of NG (78% ± 4%) than in G (60% ± 4%) systems. This result indicates that the GV of G systems has a different composition compared to that of NG systems.

(4) Seven (of nine) parameters exhibit, for all samples, the evolutionary sequence: $\mathrm{SF} \rightarrow \mathrm{GV_1} \rightarrow \mathrm{GV_2} \rightarrow \mathrm{PAS}$, with significant differences of galaxies between these evolutionary stages. We also find a strong evolutionary segregation between bright and faint galaxies, independently on whether the galaxies are located in G or NG systems. This result indicates that the mechanisms of quenching are more dependent on the luminosity (or mass) of galaxies, which agrees with several studies arguing in favor of stellar mass as the main driver of galaxy evolution (e.g. Peng et al. 2010; Contini et al. 2019). Additional mechanisms are also required because mass-quenching alone cannot explain the morphological-structural transformations in the build up of passive galaxies or the various trends we have found.

(5) Fractions of galaxies E and S0 increase while those of Sab and Scd decrease along the evolutionary sequence. We also find that GV1 is dominated by a mixture of S0 and Sab, while GV2 is more populated by S0 galaxies (and E galaxies in GB and NGB samples). This indicates that morphological transformations of spiral galaxies into S0s must happen due to environmental effects, both in G and NG systems.

(6) VDPs of bright galaxies in G and NG systems are quite different. In G systems all populations present monotonic decreasing profiles, with differences only in the central region of the clusters; while in NG systems PAS and GV populations seem to be dynamically disturbed. Another important difference refers to the SF population in NG systems. Both bright and faint galaxies have decreasing VDP, indicating the presence of infall, but the bright ones correspond to Sab objects, while the faint are Scd galaxies.

(7) Faint Scd in NG systems present asymmetries at least 3σ above the mean asymmetry in the field, suggesting they may be experiencing interactions that affect their shape, namely harassment, ram-pressure, and minor-mergers may be the mechanisms operating as the Scd galaxies feel the global cluster potential and start interacting with the cluster members.

(8) Items (6) and (7) indicate that the main difference

regarding the distinction of galaxy evolution in G and NG systems refers to the morphology of galaxies infalling onto these systems.

ACKNOWLEDGEMENTS

We thank the referee for useful suggestions. We also thank R. Dupke for the critical reading of the work. ALBR thanks the support of CNPq, grant 311932/2017-7. RRdC acknowledges financial support from FAPESP through grant 2014/11156-4. SBR thanks the support of FAPERGS. PAAL thanks the support of CNPq, grant 309398/2018-5. This study was financed in part by the Coordenação de Aperfeiçoamento de Pessoal de Nível Superior - Brasil (CAPES) - Finance Code 001.

This research has made use of the SAO/NASA Astrophysics Data System, the NASA/IPAC Extragalactic Database (NED) and the ESA Sky tool (sky.esa.int/). Funding for the SDSS and SDSS-II was provided by the Alfred P. Sloan Foundation, the Participating Institutions, the National Science Foundation, the U.S. Department of Energy, the National Aeronautics and Space Administration, the Japanese Monbukagakusho, the Max Planck Society, and the Higher Education Funding Council for England. A list of participating institutions can be obtained from the SDSS Web Site http://www.sdss.org/.

REFERENCES

Abramson L. E., Kelson D. D., Dressler A., Poggianti B., Gladders M. D., Oemler Augustus J., Vulcani B., 2014, ApJ, 785, L36
Adami C., Biviano A., Mazure A., 1998, A&A, 331, 439
Aguerri J. A. L., Sánchez-Janssen R., Muñoz-Tuñón C., 2007, A&A, 471, 17
Allen S. W., Rapetti D. A., Schmidt R. W., Ebeling H., Morris R. G., Fabian A. C., 2008, MNRAS, 383, 879
Amari S., 1985
Andrade A., Ribeiro A. L. B., Rosa R. R., 2006, Physica D: Nonlinear Phenomena, 223, 139
Bait O., Barway S., Wadadekar Y., 2017, Monthly Notices of the Royal Astronomical Society, 471, 2687
Barchi P. H., et al., 2020, Astronomy and Computing, 30, 100334
Bartalucci I., Arnaud M., Pratt G. W., Démoclès J., Lovisari L., 2019, arXiv e-prints, p. arXiv:1906.02339
Beers T. C., Flynn K., Gebhardt K., 1990, AJ, 100, 32
Belfiore F., et al., 2018, Monthly Notices of the Royal Astronomical Society, 477, 3014
Bergond G., Zepf S. E., Romanowsky A. J., Sharples R. M., Rhode K. L., 2006, A&A, 448, 155
Bilton L. E., Pimbblet K. A., 2018, MNRAS, 481, 1507
Biviano A., Katgert P., 2004, Astronomy & Astrophysics, 424, 779
Biviano A., Katgert P., Thomas T., Adami C., 2002, A&A, 387, 8
Boselli A., Gavazzi G., 2006, Publications of the Astronomical Society of the Pacific, 118, 517
Bradford J. D., Geha M. C., Blanton M. R., 2015, The Astrophysical Journal, 809, 146
Bremer M. N., et al., 2018, MNRAS, 476, 12
Brennan R., et al., 2015, MNRAS, 451, 2933
Cava A., et al., 2017, A&A, 606, A108
Chen Y.-M., et al., 2012, MNRAS, 421, 314
Cid Fernandes R., Mateus A., Sodré L., Stasińska G., Gomes J. M., 2005, MNRAS, 358, 363
Coenda V., Martínez H. J., Muriel H., 2018, MNRAS, 473, 5617
Cohen S. A., Hickox R. C., Wegner G. A., 2015, ApJ, 806, 85
Conover W., 1999, Practical nonparametric statistics, pp 229–39
Contini E., Gu Q., Kang X., Rhee J., Yi S., 2019, The Astrophysical Journal, 882, 167
Corder G., Foreman D., 2009, Nonparametric Statistics for Non-Statisticians. John Wiley & Sons, Inc, pp 38–56
Cortese L., 2012, Astronomy & Astrophysics, 543, A132
Costa A. P., Ribeiro A. L. B., de Carvalho R. R., 2018, MNRAS, 473, L31
D'Onofrio M., Marziani P., Buson L., 2015, Frontiers in Astronomy and Space Sciences, 2, 4
Domínguez Sánchez H., Huertas-Company M., Bernardi M., Tuccillo D., Fischer J. L., 2018, MNRAS, 476, 3661
Dressler A., Abramson L., 2015, in Cappellari M., Courteau S., eds, IAU Symposium Vol. 311, Galaxy Masses as Constraints of Formation Models. pp 140–145, doi:10.1017/S1743921315003555
Eales S., de Vis P., Smith M. W. L., Appah K., Ciesla L., Duffield C., Schofield S., 2017, MNRAS, 465, 3125
Einasto M., et al., 2012, A&A, 542, A36
Fadda D., Girardi M., Giuricin G., Mardirossian F., Mezzetti M., 1996, ApJ, 473, 670
Faltenbacher A., Diemand J., 2006, Monthly Notices of the Royal Astronomical Society, 369, 1698
Fernández M. d. C. A., Yuan F., Shen S., Yin J., Chang R., Feng S., 2015, Galaxies, 3, 156
Fitchett M., Webster R., 1987, The Astrophysical Journal, 317, 653
Foëx G., 2019, arXiv e-prints, p. arXiv:1901.09198
Fontanot F., De Lucia G., Monaco P., Somerville R. S., Santini P., 2009, Monthly Notices of the Royal Astronomical Society, 397, 1776
Gallazzi A., Charlot S., Brinchmann J., White S. D. M., Tremonti C. A., 2005, MNRAS, 362, 41
Ge X., Gu Q.-S., Chen Y.-Y., Ding N., 2018, arXiv e-prints, p. arXiv:1808.01709
Girardi M., Giuricin G., Mardirossian F., Mezzetti M., Boschin W., 1998, The Astrophysical Journal, 505, 74
Giraudoux P., 2018, pgirmess: Spatial Analysis and Data Mining for Field Ecologists. `https://CRAN.R-project.org/package=pgirmess`
Gu Y., Fang G., Yuan Q., Cai Z., Wang T., 2018, The Astrophysical Journal, 855, 10
Hou A., Parker L. C., Harris W. E., Wilman D. J., 2009, ApJ, 702, 1199
Hou A., et al., 2012, MNRAS, 421, 3594
Huber P., 1981, Wiley series in probability and mathematical statistics
Kauffmann G., et al., 2003, MNRAS, 341, 33
Kauffmann G., White S. D. M., Heckman T. M., Ménard B., Brinchmann J., Charlot S., Tremonti C., Brinkmann J., 2004, MNRAS, 353, 713
Kennicutt Jr R. C., 1998, Annual Review of Astronomy and Astrophysics, 36, 189
Khim H.-g., Park J., Seo S.-W., Lee J., Smith R., Sukyoung K. Y., 2015, The Astrophysical Journal Supplement Series, 220, 3
Li I., et al., 2011, Monthly Notices of the Royal Astronomical Society, 411, 1869
Lintott C. J., et al., 2008, MNRAS, 389, 1179
Lopes P. A. A., de Carvalho R. R., Kohl-Moreira J. L., Jones C., 2009, MNRAS, 399, 2201
Lopes P. A. A., Trevisan M., Laganá T. F., Durret F., Ribeiro A. L. B., Rembold S. B., 2018, MNRAS, 478, 5473
Mamon G., Cava A., Biviano A., Moretti A., Poggianti B., Bettoni D., 2019, Astronomy & Astrophysics, 631, A131
Martin D. C., et al., 2005, The Astrophysical Journal Letters, 619, L1

Martínez H. J., Zandivarez A., 2012, MNRAS, 419, L24
Menci N., Fusco-Femiano R., 1996, ApJ, 472, 46
Mendel J. T., Simard L., Palmer M., Ellison S. L., Patton D. R., 2013, The Astrophysical Journal Supplement Series, 210, 3
Mendez A. J., Coil A. L., Lotz J., Salim S., Moustakas J., Simard L., 2011, ApJ, 736, 110
Millard S. P., 2013, EnvStats: An R Package for Environmental Statistics. Springer, New York, http://www.springer.com
Million E. T., Allen S. W., 2009, MNRAS, 399, 1307
Mohr J., Geller M., Fabricant D., Wegner G., Thorstensen J., Richstone D., 1996, arXiv preprint astro-ph/9604169
Moore B., Katz N., Lake G., Dressler A., Oemler A., 1996, nature, 379, 613
Moss C., 2006, Monthly Notices of the Royal Astronomical Society, 373, 167
Nair P. B., Abraham R. G., 2010, ApJS, 186, 427
Nascimento R. S., Lopes P. A. A., Ribeiro A. L. B., Costa A. P., Morell D. F., 2019, MNRAS, 483, L121
Neistein E., Van Den Bosch F. C., Dekel A., 2006, Monthly Notices of the Royal Astronomical Society, 372, 933
Old L., et al., 2018, Monthly Notices of the Royal Astronomical Society, 475, 853
Peng Y.-j., et al., 2010, ApJ, 721, 193
Phillipps S., et al., 2019, Monthly Notices of the Royal Astronomical Society, 485, 5559
Pimbblet K. A., Penny S. J., Davies R. L., 2014, MNRAS, 438, 3049
Plionis M., 2004, Proceedings of the International Astronomical Union, 2004, 19
Plionis M., Benoist C., Maurogordato S., Ferrari C., Basilakos S., 2003, ApJ, 594, 144
Ribeiro A. L. B., Lopes P. A. A., Trevisan M., 2010, MNRAS, 409, L124
Ribeiro A. L. B., Lopes P. A. A., Trevisan M., 2011, MNRAS, 413, L81
Ribeiro A. L. B., de Carvalho R. R., Trevisan M., Capelato H. V., La Barbera F., Lopes P. A. A., Schilling A. C., 2013a, MNRAS, 434, 784
Ribeiro A. L. B., Lopes P. A. A., Rembold S. B., 2013b, A&A, 556, A74
Roberts I. D., Parker L. C., 2017, MNRAS, 467, 3268
Roberts I. D., Parker L. C., Hlavacek-Larrondo J., 2018a, MNRAS, 475, 4704
Roberts I. D., Parker L. C., Hlavacek-Larrondo J., 2018b, Monthly Notices of the Royal Astronomical Society, 475, 4704
Roberts I. D., Parker L. C., Brown T., Joshi G. D., Hlavacek-Larrondo J., Wadsley J., 2019, The Astrophysical Journal, 873, 42
Rood H. J., Page T. L., Kintner E. C., King I. R., 1972, ApJ, 175, 627
Rosa R. R., Sharma A., Valdivia J., 1999, International Journal of Modern Physics C, 10, 147
Rosa R. R., et al., 2018, MNRAS, 477, L101
Rossetti M., et al., 2016, MNRAS, 457, 4515
Salim S., 2014, Serbian Astronomical Journal, 189, 1
Schiminovich D., et al., 2007, The Astrophysical Journal Supplement Series, 173, 315
Scrucca L., Fop M., Murphy T. B., Raftery A. E., 2016, The R Journal, 8, 205
Signorell A., et al., 2016, R package version 0.99, 18
Simard L., Mendel J. T., Patton D. R., Ellison S. L., McConnachie A. W., 2011, The Astrophysical Journal Supplement Series, 196, 11
Soares N. R., Rembold S. B., 2019, MNRAS, 483, 4354
Sodre Laerte J., Capelato H. V., Steiner J. E., Mazure A., 1989, AJ, 97, 1279
Tammann G. A., 1972, A&A, 21, 355
Tempel E., Tuvikene T., Kipper R., Libeskind N. I., 2017, Astronomy & Astrophysics, 602, A100
Wen Z. L., Han J. L., 2013, MNRAS, 436, 275
Wetzel A. R., Tinker J. L., Conroy C., 2012, MNRAS, 424, 232
Willett K. W., et al., 2013, MNRAS, 435, 2835
Wyder T. K., et al., 2007, ApJS, 173, 293
Yahil A., Vidal N., 1977, The Astrophysical Journal, 214, 347
Yang X., Mo H. J., van den Bosch F. C., Jing Y. P., 2005, MNRAS, 356, 1293
Yang X., Mo H. J., van den Bosch F. C., Pasquali A., Li C., Barden M., 2007, ApJ, 671, 153
Yang H. Y. K., Bhattacharya S., Ricker P. M., 2010, ApJ, 725, 1124
Yip C. W., et al., 2004, AJ, 128, 585
York D. G., et al., 2000, AJ, 120, 1579
de Carvalho R. R., Ribeiro A. L. B., Stalder D. H., Rosa R. R., Costa A. P., Moura T. C., 2017, AJ, 154, 96
de Carvalho R., Costa A., Moura T., Ribeiro A., 2019, Monthly Notices of the Royal Astronomical Society: Letters, 487, L86

This paper has been typeset from a TEX/LATEX file prepared by the author.